JOURNAL OF CATALYSIS 149, 61–69 (1994)

Preparation of Iridium Clusters in Zeolite Y via Cation Exchange: EXAFS, Xenon Adsorption, and ^{129}Xe NMR Studies

Chanho Pak, Sung June Cho, Jeong Yong Lee,* and Ryong Ryoo[1]

*Department of Chemistry and Center for Molecular Science and *Department of Electronic Materials Science and Engineering, Korea Advanced Institute of Science and Technology, Taeduk Science Town, Taejon, 305-701 Korea*

Received November 8, 1993; revised March 22, 1994

The conversion of $[Ir(NH_3)_5Cl]^{2+}$ and $[Ir(NH_3)_5(H_2O)]^{3+}$ to 1-nm Ir clusters entrapped in the supercages of NaY zeolite has been investigated by using ^{129}Xe NMR spectroscopy, xenon adsorption, and extended X-ray absorption fine structure. The cation exchange with $[Ir(NH_3)_5Cl]^{2+}$ was achieved by slurring NaY in an aqueous solution of $[Ir(NH_3)_5Cl]Cl_2$ at room temperature. The cation exchange with $[Ir(NH_3)_5(H_2O)]^{3+}$ employed either an aqueous solution of $[Ir(NH_3)_5(H_2O)](ClO_4)_3$ at room temperature or an aqueous solution of $IrCl_3$ containing NH_3 at a temperature of 330 K. This paper reports very distinctive pretreatment requirements for the transformation of these two ionic precursors to 1-nm Ir clusters in the zeolite supercages: activation in O_2 flow at 573 K is required in the case of $[Ir(NH_3)_5Cl]^{2+}$, while outgassing at 473 K is sufficient in the case of $[Ir(NH_3)_5(H_2O)]^{3+}$, prior to the final reduction with H_2. This second method, which has not been previously described, provides a convenient route for the preparation of Ir clusters in zeolites without using an oxidative treatment, and avoiding Cl-containing species. Furthermore, results from ^{129}Xe NMR and xenon adsorption measurements indicate that the cluster size is substantially smaller than that in the case of $[Ir(NH_3)_5Cl]^{2+}$. © 1994 Academic Press, Inc.

INTRODUCTION

Metal clusters in zeolite cages attract much attention as model catalytic materials because of their very high metal dispersion and structural uniformity. The metal is loaded onto the zeolite by cation exchange, gas adsorption, or liquid impregnation using a suitable precursor. However, it is not straightforward to obtain a uniform cluster size in the zeolite cage. The metal often migrates from the cages to the external surface of the zeolite crystal during reduction, or forms large agglomerates imbedded within the zeolite matrix. It is therefore important to investigate the effect of sample pretreatment on cluster size and morphology.

Previous studies on the preparation of Ir clusters in NaY zeolite cages (Ir/NaY) used ion exchange of $[Ir(NH_3)_5Cl]^{2+}$ (1–4) or impregnation of a carbonyl complex (5–7). In the case of $[Ir(NH_3)_5Cl]^{2+}$, it is agreed that the ion-exchanged Ir species in the zeolite should be activated by flowing O_2 at high temperatures, e.g., 523 K, prior to reduction with H_2. The reduction of the Ir/NaY precursor by H_2 without the activation treatment is known to lead to the formation of 2–3 nm agglomerates embedded in the zeolite matrix.

Recently, we have studied by ^{129}Xe NMR spectroscopy the formation of Ir and PtIr clusters in the supercages of NaY zeolite using ion exchange of $Pt(NH_3)_4^{2+}$ and $[Ir(NH_3)_5Cl]^{2+}$ (4). The chemical shift of xenon was investigated as a probe for the formation of a bimetallic cluster. Thus, our earlier paper was focused on the chemical shift effects due to the combination of Pt and Ir in the same cluster. Comparatively, this paper presents the effects of the Ir/NaY sample treatments on the chemical shift of xenon. Extended X-ray absorption fine structure (EXAFS) (8) was also used for the characterization of Ir species which caused the chemical shift effects. A xenon adsorption technique was also used to estimate the Ir cluster size. A better understanding of the chemistry in the Ir/NaY preparation method, and thus an improvement of the procedure, was the aim throughout this investigation.

EXPERIMENTAL

NaY zeolite was prepared as reported earlier (9). $[Ir(NH_3)_5Cl]Cl_2$ was synthesized by starting with $IrCl_3$ and three equivalents of KCl instead of $K_3[IrCl_6] \cdot 3H_2O$, following a standard procedure in the literature (10). The product was identified by comparing the UV absorption spectrum with commercial $[Ir(NH_3)_5Cl]Cl_2$ (Alpha, 50.10% Ir).

Two kinds of Ir/NaY precursors were prepared. One sample was obtained by stirring 2.00 g (in dehydrated weight) of the zeolite powder in 300 ml of aqueous solution of 1.1×10^{-3} *M* $[Ir(NH_3)_5Cl]Cl_2$ for 12 h at room temperature (RT) (1). It is designated Ir/NaY–Cl. The other sam-

[1] To whom correspondence should be addressed.

0021-9517/94 $6.00
Copyright © 1994 by Academic Press, Inc.
All rights of reproduction in any form reserved.

TABLE 1

Chemical Analysis of the Ir/NaY Samples

Sample	wt% Ir	wt% Cl	Cl/Ir
Ir/NaY–Cl	11.9	2.15	0.98
Ir/NaY–Aq	12.1	0.13	0.06
$[Ir(NH_3)_5(H_2O)]^{3+}$–NaY	10.8	0.06	0.03

ple was prepared as follows: 0.332 g of $IrCl_3$ (Johnson Matthey, 51.26% Ir) was dissolved in 300 ml of concentrated aqueous ammonia solution at RT. The color of this solution was yellow. NaY zeolite powder (2.00 g in dehydrated weight) was added to the solution. The solution was then heated to 330 K. The color turned faint pink after stirring for 12 h at 330 K under a reflux condenser, and afterward gradually colorless when the stirring was continued for 3 days. This period could be reduced substantially by adding to the solution a small amount of NaOH as a catalyst. The zeolite sample was then filtered, washed with doubly distilled water, and dried in vacuum oven at RT. It is designated Ir/NaY–Aq. Analysis for iridium and chlorine content in the precursors was carried out by proton-induced emission of X-ray fluorescence (using 2.4-MeV protons accelerated by NEC SSDH-2, and equipped with a Si(Li) X-ray detector). The sodium content of the supernatant solution was analyzed by atomic absorption spectroscopy (Instrumental Analysis, Video 12) after the Ir/NaY was filtered off. Results for chemical analysis are summarized in Table 1. The Ir content from the elemental analysis corresponds to 7.9 Ir atoms per unit cell for Ir/NaY–Cl and 8.0 for IrNaY–Aq. Approximately, three Na^+ ions per Ir in the zeolite were released from NaY into the ammonia solution.

The sample treatment, xenon adsorption measurements, and ^{129}Xe NMR experiment were performed in the same way as reported recently for Pt/NaY (9, 11). For the EXAFS measurement of an unreduced sample, about 0.15 g of the sample powder was pressed into a self-supporting wafer of 10 mm diameter. The sample was evacuated under 1×10^{-3} Pa for 2 h at RT in a Pyrex U-tube flow reactor that was joined to a Pyrex cell having Kapton (Du Pont) windows. The sample wafer was transferred to the EXAFS cell by tilting the reactor. Then, the cell was sealed off from the reactor with flame under a He atmosphere. For the EXAFS of reduced Ir/NaY sample, the EXAFS cell was sealed off under a H_2 atmosphere after the sample was reduced again in the reactor by flowing H_2 at 573 K. The X-ray absorption measurement was carried out at the Ir L_{III} edge at RT using Beam Line 10B at the Photon Factory in Tsukuba. The injection beam energy was 2.5 GeV. The ring current was maintained as 250–350 mA. The monochromator was a Si(311) channel cut with a typical resolution $\Delta E/E = 1 \times 10^{-4}$ at the Ir L_{III} edge. The energy steps in the absorption edge and EXAFS regions were 0.5 and 2.3 eV, respectively. The intensity of X-ray was measured by using a gas ionization chamber. Detector gases for the incident and transmitted X-ray intensities were 85% N_2–15% Ar and 75% N_2–25% Ar, respectively. Analysis of the X-ray absorption data was carried out by standard methods (8) using the UWXAFS 2.0 code distributed by the University of Washington (12). An Ir/NaY sample containing 50–100 nm Ir clusters on the external surface of a zeolite crystal was prepared by reduction of Ir/NaY–Cl at 573 K after the activation at 773 K, in order to use it as a reference for EXAFS curve fitting.

For transmission electron microscopy, a suspension of the sample powder in methanol was dropped onto microporous carbon grid and allowed to dry. Micrographs of the thin edges of the zeolite crystal (~1 μm) were taken with a JEM 2000-EX (JEOL) instrument operating at 200 keV.

RESULTS AND DISCUSSION

Structure of Cation-Exchanged Species

Figure 1 shows EXAFS oscillations and the Fourier transforms of the Ir/NaY–Cl precursor and $[Ir(NH_3)_5Cl]Cl_2$ powder. The Fourier transformation was performed from a region of wave vector $0.3 < k < 1.5$ nm^{-1} into R space, after being weighted by k^3. The main features of the Fourier transform of Ir/NaY–Cl for $R <$ 0.25 nm are identical to those of the $[Ir(NH_3)_5Cl]Cl_2$ powder. Small peaks beyond 0.25 nm may differ due to the two Cl^- anions in the outer sphere, multiple scattering effects and possibly due to noise. These EXAFS features

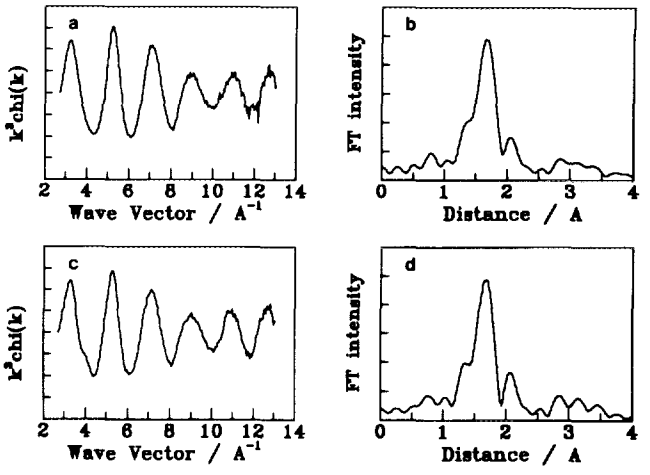

FIG. 1. Normalized EXAFS oscillation, $k^3 \chi(k)$ vs k at 300 K and the corresponding Fourier transforms: (a, b) Ir/NaY–Cl and (c, d) $[Ir(NH_3)_5Cl]Cl_2$ powder.

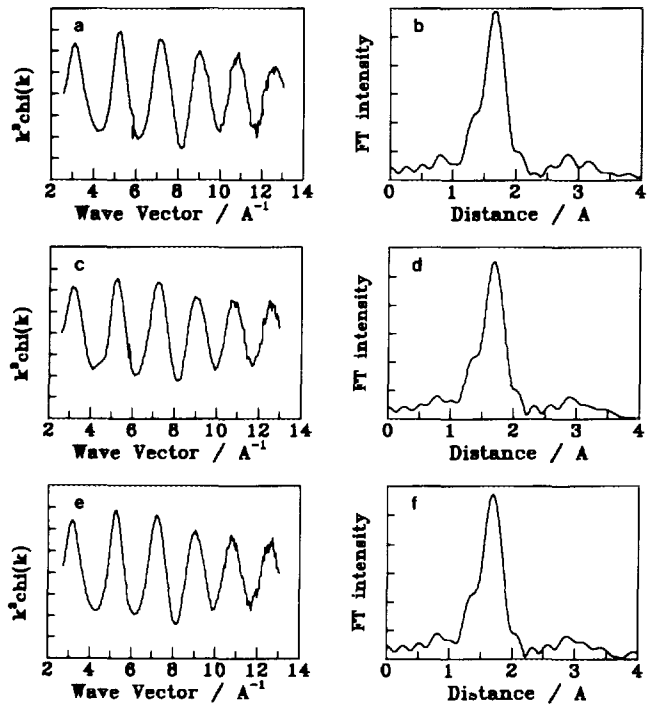

FIG. 2. Normalized EXAFS oscillation, $k^3\chi(k)$ vs k at 300 K and the corresponding Fourier transforms: (a, b) Ir/NaY–Aq (c, d) $[Ir(NH_3)_5(H_2O)](ClO_4)_3$ powder, and (e, f) $[Ir(NH_3)_5(H_2O)]^{3+}$–NaY.

indicate that the inner sphere ligands of the two species are identical: five NH_3 and one Cl^-. No further quantitative data analysis seems necessary to support this conclusion, since the chemical analysis in Table 1 further confirms that the Ir species in Ir/NaY–Cl contains one Cl per Ir. Certainly, a ligand exchange in aqueous solution by $[Ir(NH_3)_5Cl]^{2+} + H_2O \rightleftarrows [Ir(NH_3)_5(H_2O)]^{3+} + Cl^-$ did not occur under our experimental condition. Thus, the $[Ir(NH_3)_5Cl]^{2+}$ ion was exchanged into NaY zeolite without changing the inner-sphere ligands in $[Ir(NH_3)_5Cl]Cl_2$.

On the other hand, EXAFS data for Ir/NaY–Aq shown in Fig. 2 are very different from $[Ir(NH_3)_5Cl]^{2+}$. Chemical analysis of Ir/NaY–Aq for chlorine indicated that it did not contain a Cl^- ligand. Moreover, the Na^+ analysis of the supernatant solution obtained after the preparation of the precursor indicated that three Na^+ ions per Ir were released from NaY into the solution by ion exchange of the iridium species. Therefore, the formula of the iridium species was assumed to be $[Ir(NH_3)_m(H_2O)_{6-m}]^{3+}$. To complete the structural formula, the EXAFS spectrum in k space was Fourier filtered by performing an inverse Fourier transformation from $0.12 < R < 0.23$ nm to $0.30 < k < 1.50$ nm^{-1}. A detailed curve fitting analysis of the Fourier filtered EXAFS oscillation ($\chi(k)$) was performed with a theoretical reference $\chi(k)$ for Ir–N and Ir–O pairs, which were generated by FEFF3 code taking into account single scattering, many body, and curved wave effects (13). The structural parameters used in the $\chi(k)$ generation are included in Table 2. The EXAFS curve fitting for Ir/NaY–Aq was carried out while the phase shift adjustment parameters, ΔE_0 for Ir–N and Ir–O pairs (denoted as ΔE_0^{Ir-N} and ΔE_0^{Ir-O}, respectively), were drifted independently. At each point of (ΔE_0^{Ir-N}, ΔE_0^{Ir-O}), a value of m (i.e., the number of NH_3 ligands) was obtained to give the best curve fit. The normalized error obtained in the curve fit is plotted against the ΔE_0^{Ir-N} and ΔE_0^{Ir-O}, as shown in Fig. 3. The error reached a minimum point when ΔE_0^{Ir-N} and ΔE_0^{Ir-O} were -10 and -2 eV, respectively. At this point, the best fit m was 4.7. Thus, the curve fitting analysis under the above structural assumption best agreed with a formula $[Ir(NH_3)_5(H_2O)]^{3+}$. Bond distances for Ir–N and Ir–O obtained from the best curve fit were 0.208 and 0.193 nm, respectively. This curve fitting result has been confirmed in R space by comparing Fourier transforms of the experimental $k^3\chi(k)$ and a theoretical $k^3\chi(k)$, which was generated by FEFF5 code taking into account multiple scattering, many body, and spherical wave effects (14), in Fig. 4.

Normally, it is difficult in EXAFS data analysis to distinguish back scattering from light atoms like N and O. In the present case with $[Ir(NH_3)_5(H_2O)]^{3+}$, the structural

TABLE 2

Structural Parameters for the Generation of Reference EXAFS and Samples Obtained from EXAFS

Sample	Atomic pair	R (nm)[a]	N[b]	σ^2 (pm^2)[c]
Reference[d]	Ir–N	0.210	6	37
Reference[d]	Ir–O	0.200	6	37
Reference[e]	Ir–Ir	0.271	12	0
Ir/NaY–Aq[f]	Ir–N	0.208	4.7	52
	Ir–O	0.193	1.2	83
Ir/NaY–Cl[g]	Ir–O	0.197	5.5	103
Ir/NaY–Cl[h]	Ir–O	0.198	6.0	27
Ir/NaY–Cl[i]	Ir–Ir	0.269	8.4	35
Ir/NaY–Aq[j]	Ir–Ir	0.270	7.7	30

[a] The nearest neighbor distance with ±0.002 nm.
[b] The nearest neighbor coordination number with ±1.0 for samples.
[c] The Debye–Waller factor.
[d] Each reference $\chi(k)$ oscillation was obtained from a theoretical calculation using FEFF-3 code, with the listed R, N, and σ^2 values. The amplitude reduction factor, $S_0^2 = 0.89$, was obtained from EXAFS curve fitting for the Ir/NaY sample in Fig. 7c. This value was also used in the $\chi(k)$ generation.
[e] An experimentally measured reference EXAFS from Ir/NaY in Fig. 7c. R and N are value for bulk Ir.
[f] Precursor state.
[g] After activation at 573 K.
[h] After activation at 773 K.
[i] Reduced at 573 K after activation at 573 K.
[j] Reduced at 573 K after evacuation at 723 K.

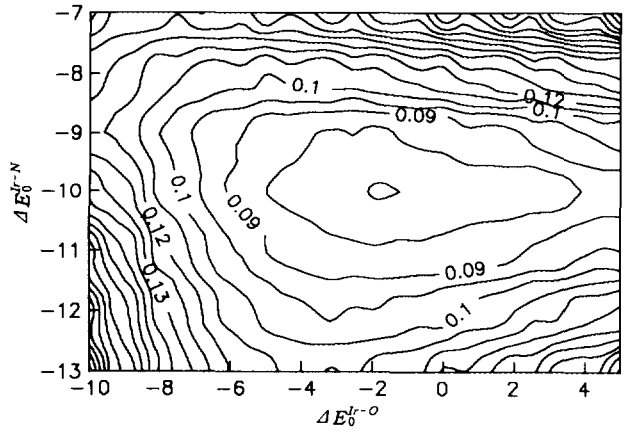

FIG. 3. Contour map of normalized error obtained in the EXAFS curve fit for Ir/NaY–Aq, plotted against the variation of ΔE_0^{Ir-N} and ΔE_0^{Ir-O}, respectively.

formula was confirmed with $[Ir(NH_3)_5(H_2O)](ClO_4)_3$ which was synthesized according to a produce in the literature (10). This compound was dissolved in water. The solution was stirred with NaY zeolite overnight at RT for the ion exchange of $[Ir(NH_3)_5(H_2O)]^{3+}$. The ClO_4^- anions in this complex should exist in the outer ligand sphere, and therefore the Cl^--containing anions are removed by washing after the ion exchange. The iridium zeolite ($[Ir(NH_3)_5(H_2O)]^{3+}$–NaY) thus obtained indeed gave identical EXAFS data to Ir/NaY–Aq and $[Ir(NH_3)_5(H_2O)](ClO_4)_3$ powder, as shown in Fig. 2. Furthermore, this $[Ir(NH_3)_5(H_2O)]^{3+}$–NaY sample showed same characteristic ^{129}Xe NMR spectrum and xenon adsorption isotherm as Ir/NaY–Aq, throughout the high-temperature evacuation and reduction treatments discussed below.

Effect of Sample Pretreatment

The ^{129}Xe NMR spectra of NaY and Ir/NaY obtained under 53.3 kPa at 296 K are shown in Fig. 5. The chemical shift (δ) of Ir/NaY increased remarkably by the Ir loading on NaY zeolite. The chemical shift is well known to be affected by the physicochemical environment of zeolite cages, due to, e.g., xenon adsorption on metal clusters, xenon–ion interactions, and collisions between xenon and the zeolite framework. Since our attention was focused on the cluster formation, all other effects were eliminated from the δ difference between Ir/NaY and NaY by measuring a difference caused by H chemisorption on Ir/NaY. First, the Ir/NaY sample was allowed to contact with 1 atm H_2 for longer than 30 min at RT. Subsequently, the gaseous H_2 and reversibly adsorbed H were removed over 1 h under vacuum of 1×10^{-3} Pa at RT. The H irreversibly chemisorbed on the metal clusters under this condition was regarded to inhibit most of the Xe–cluster interaction, decreasing δ (9, 11, 15, 16). However, the other effects coming from cationic or oxide species of Ir were negligible since the species did not chemisorb H under these conditions. Thus the δ difference (Δ δ) between a "clean" Ir/NaY sample and that after H chemisorption was used in this work to characterize the Ir clusters in NaY.

The Ir/NaY–Cl precursor was activated in flowing O_2 at various temperatures, and then subjected to the reduction with H_2. The O_2 flow rate was adjusted to be 1 liter min^{-1} g^{-1}. The activation temperature was increased at 0.5 K min^{-1} from RT to a given temperature and maintained there for 2 h. Subsequently, the sample was evacuated for 2 h at RT. The reduction was performed in flowing H_2 (>200 ml min^{-1} g^{-1}), while the temperature was raised at a rate of 1.25 K min^{-1} from RT to 573 K and maintained

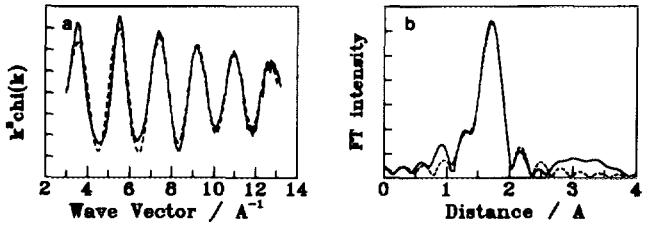

FIG. 4. A comparision of (a) the EXAFS oscillations ($k^3 \chi(k)$) and (b) the corresponding Fourier transforms for Ir/NaY–Aq between experimental (solid line) and fitted (dashed line).

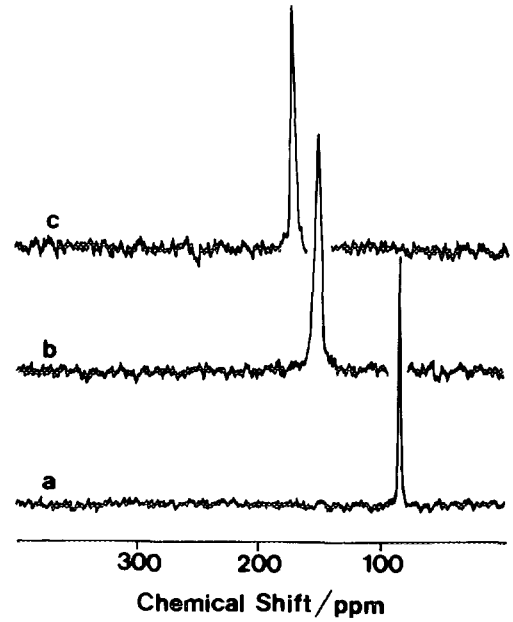

FIG. 5. ^{129}Xe NMR spectra at 296 K and 53.3 kPa of adsorbed xenon: (a) NaY evacuated at 673 K, (b) Ir/NaY–Cl reduced at 573 K after activation at 573 K, and (c) Ir/NaY–Aq reduced at 573 K after evacuation at 673 K.

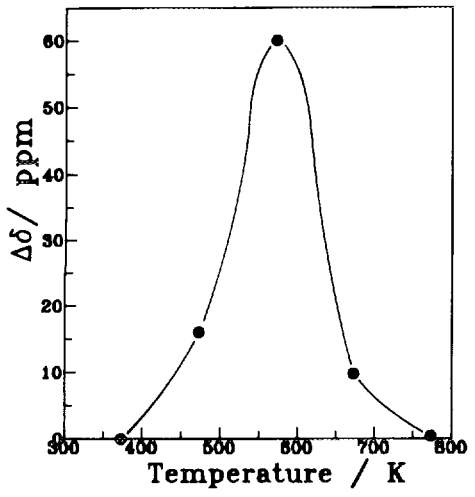

FIG. 6. Chemical shift difference (Δ δ) due to H chemisorption in the ^{129}Xe NMR spectra of adsorbed xenon on reduced Ir/NaY–Cl, plotted against the activation temperature at a xenon pressure of 53.3 kPa.

there for 2 h. The sample was subsequently evacuated for 2 h at 673 K. The Δ δ of this sample due to H chemisorption was measured by the aforementioned way. The measured value under 53.3 kPa Xe pressure at 296 K is plotted against the given activation temperature (T_{act}) in Fig. 6. A Δ δ maximum at about 570 K indicates that the highest metal dispersion was achieved under this condition.

The transmission electron micrographs in Fig. 7 are consistent with the Δ δ vs T_{act} curve in Fig. 6. Figure 7a shows that the sample reduction after activation at 573 K gave mainly small Ir clusters with ca. 1–2 nm size. Figure 7b indicates that the Ir atoms agglomerated into ca. 3–7 nm particles embedded within the zeolite crystal when the Ir reduction was performed without the O_2 treatment. This is consistent with earlier results (3). Interestingly, the agglomerate size did not change significantly, although the heating rate for the direct reduction of Ir with H_2 was changed over a wide range, 0.67–3.3 K min^{-1}.

As compared to the above direct reduction, it has been confirmed from Fig. 7c that large Ir particles were obtained at the external surface of the zeolite crystals when Ir was reduced after the Ir/NaY–Cl precursor was activated with O_2 at 773 K. Such Ir sintering with increasing activation temperature to above 573 K agrees with the high volatility of IrO_2 under O_2 atmosphere. It seemed that the IrO_2 evaporated from the pore of zeolite to the external surface of zeolite crystal. A film of blackish IrO_2 was formed on the inner wall at downstream of a Pyrex reactor during the precursor heating to above 673 K in O_2. This property of Ir is similar to sintering Ru/NaY in O_2 (15), but to a much lesser extent.

EXAFS spectra and powder XRD patterns of Ir/NaY–Cl were obtained after activation at 573 and 773 K, in order to investigate structural changes in the Ir species due to activation in O_2. A large IrO_2 phase with a rutile structure (17) was clearly detected with XRD in the case of activation at 773 K: three peaks at 2 θ = 27.6, 34.5, and 53.8° in XRD. Reduction of this large IrO_2 cluster in H_2 gave the 50–100 nm Ir cluster shown in Fig. 7c. In agreement with IrO_2, Fourier transforms of the EXAFS spectra in Fig. 8 show an intense peak for an Ir–O bond around 0.19 nm after treatment with O_2. A similar peak at 0.19 nm also appeared in Fourier transform of EXAFS when Ir/NaY–Cl was activated at 573 K. However, the peak was much less intense and broader. Moreover, the IrO_2 phase was not detectable with XRD in this case. Probably, a very small cluster of IrO_2 was obtained within the supercage. The small IrO_2 cluster is believed to be transformed into a 1-nm Ir cluster by subsequent reduction within the supercage. The curve fitting was carried out for up to the second shell in both R and k spaces using UWXAFS 2.0 taking into account multiple scattering up to 3, many body, and curved wave effects (14). The structural parameters are given in Table 2. These parameters are very similar to the values for IrO_2 with a rutile structure.

The effect of the evacuation of Ir/NaY precursors has been investigated by using ^{129}Xe NMR spectroscopy in the following ways. The Ir/NaY precursors were first evacuated at various temperatures and subsequently subjected to reduction. The evacuation temperature was increased at 0.83 K min^{-1} from RT to a given temperature and maintained there for 2 h. Reduction was performed at 573 K. The, Δ δ in ^{129}Xe NMR for these samples due to irreversible H chemisorption was measured at 296 K. This result is plotted against the evacuation temperature in Fig. 9. The Ir/NaY–Cl sample gave very small Δ δ over the entire range of evacuation temperature, which is consistent with the above result that the Ir atoms agglomerated into 3–7 nm clusters if reduced without precursor activation in O_2. Interestingly, the Δ δ of Ir/NaY–Aq is much larger than that of Ir/NaY–Cl over the entire temperature range. Figure 7d shows a transmission electron micrograph for Ir/NaY–Aq after evacuation at 723 K and subsequent reduction with H_2 at 573 K. Small cluster sizes with 1–2 nm clarify that, unlike Ir/NaY–Cl, the Ir/NaY–Aq precursor may be used to obtain a small cluster by such an evacuation–reduction procedure.

Furthermore, the result for Ir/NaY–Aq in Fig. 9 shows a peculiar maximum at 473 K. The value of Δ δ at this point is much greater than the maximum in Fig. 3, which was obtained from the Ir/NaY–Cl precursor according to conventional O_2-activation procedure. This anomalous maximum at 473 K has been repeated by two investigators working in this laboratory with an ammonia solution of $IrCl_3$ and an aqueous solution of $[Ir(NH_3)_5(H_2O)](ClO_4)_3$ independently. The Ir/NaY–Aq sample thus obtained

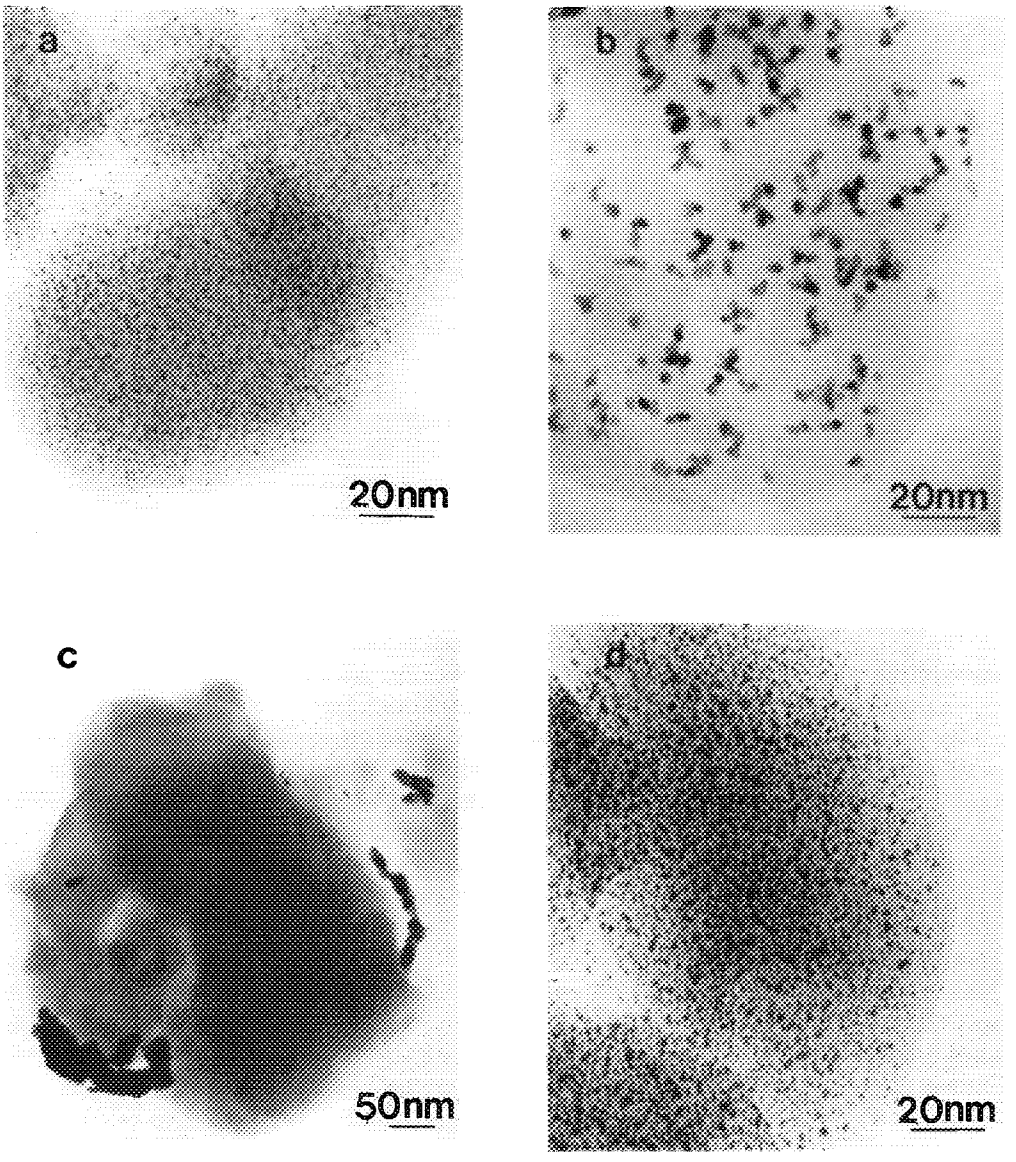

FIG. 7. Transmission electron micrographs: (a) Ir/NaY–Cl reduced at 573 K after activation at 573 K, (b) Ir/NaY–Cl reduced at 673 K without activation, (c) Ir/NaY–Cl reduced at 573 K after activation at 773 K, and (d) Ir/NaY–Aq reduced at 573 K after evacuation at 723 K.

contained a significantly smaller cluster than Ir/NaY–Cl, and chemisorbed much more H/Ir, as compared in Table 3. Further works on the EXAFS, TEM, and H chemisorption seem to be necessary to clarify this anomaly.

A sharp increase in ^{129}Xe NMR δ was obtained at 600 K in a plot of δ vs evacuation temperature for Ir/NaY–Aq without further reduction. This increase in δ is very similar to the case of Ru/NaY, which was attributed to autoreduction of Ru due to NH_3 ligand (15). Formation of a reduced Ir–Ir bond with a bond distance 0.270 nm was also indicated from Fourier transforms of EXAFS spectra of Ir/NaY–Aq evacuated above 573 K. Such autoreduction of Ir during precursor evacuation was quantitatively determined by H_2 uptake, as explained below. First, consumption of H_2 was measured volumetrically during the reduction with static H_2 at 573 K after Ir/NaY–Aq was evacuated at 773 K. Then, the H_2 uptake was measured again after subsequent evacuation of this sample at 673 K. The difference between these H_2 uptakes may be regarded as used for Ir reduction, and then it corresponds to only 10% H_2 required for complete reduction from Ir(III) to Ir(0). In this case of evacuation at 773 K, the degree of autoreduction amounted to 90%. This is also very similar to H_2 uptake due to autoreduction of a ruthe-

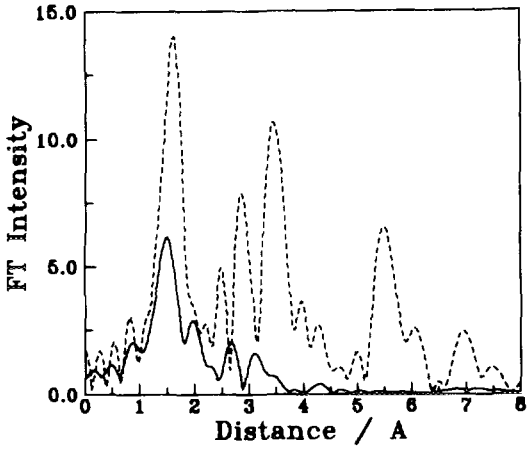

FIG. 8. Fourier transforms of EXAFS of Ir/NaY–Cl after activation at (–) 573 K and (---) 773 K.

nium red complex ion to a small Ru cluster in NaY zeolite during evacuation at 673 K (15). A similar result of H_2 uptake was obtained from Ir/NaY–Cl. However, δ did not increase due to the evacuation at high temperature. Moreover, large agglomerates of Ir were seen in the transmission electron micrograph. Thus the results for Ir/NaY–Cl are very different from the behavior of Ir/NaY–Aq. The difference between Ir/NaY–Cl and Ir/NaY–Aq may be attributed to Cl^- that may cause migration of Ir species during reduction.

Metal Cluster Size from Xenon Adsorption Measurement

Figure 10 shows the difference between xenon adsorption isotherm obtained at 296 K from a "clean" Ir/NaY sample and that from the same sample measured after H chemisorption as for the above Δ δ measurement. This result with Ir/NaY is very similar to earlier Xe adsorption isotherms for Pt/NaY (9, 11), Ru/NaY (15), Pd/NaY (16), etc. The adsorption changes due to H chemisorption are known to occur because the chemisorbed H inhibits strong Xe adsorption on the Ir clusters (9, 11, 15, 16). Thus the isotherm difference in Fig. 10 provides the Xe adsorption isotherm on "clean" Ir clusters.

Figure 10 indicates that the Xe adsorption on "clean" Ir cluster became nearly saturated at 10 kPa, whereas it almost increased on the zeolite surface according to the Henry's law. Xenon adsorption quantity for saturation on the Ir clusters can be obtained by extrapolating the

TABLE 3

Xenon Adsorption Quantity for Saturation on the Ir Cluster, the Average Number of Iridium Atoms per Cluster Obtained from the Xenon Adsorption Measurement and H Chemisorption

Sample	Treatment	Xe/Ir[a]	n^b	H_{total}/Ir^c
Ir/NaY–Cl	Activation at 573 K Reduction at 573 K	0.083	48	1.6
Ir/NaY–Aq	Evacuation at 723 K Reduction at 573 K	0.076	52	1.2
Ir/NaY–Aq	Evacuation at 473 K Reduction at 573 K	0.133	30	2.1

[a] Xenon adsorption difference due to hydrogen chemisorption on Ir/NaY, extrapolated from high-pressure region above 10 kPa to zero pressure (see Fig. 10).

[b] The number of Ir atoms per cluster, obtained from Xe/Ir ratio using Fig. 12.

[c] Determined by extrapolating the total adsorption isotherm between 10 and 50 kPa to zero pressure.

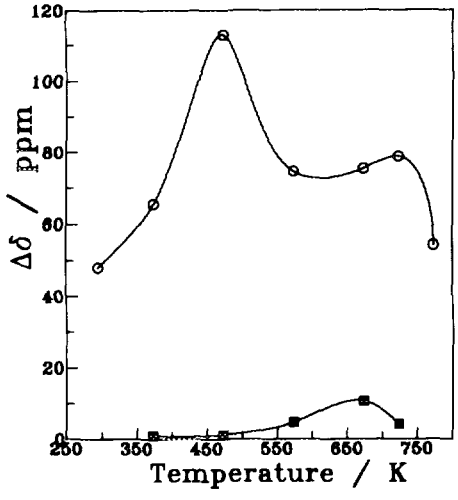

FIG. 9. Chemical shift difference (Δ δ) due to H chemisorption on Ir/NaY after reduction at 573 K, plotted against the evacuation temperature: Ir/NaY–Cl (■) and Ir/NaY–Aq (○).

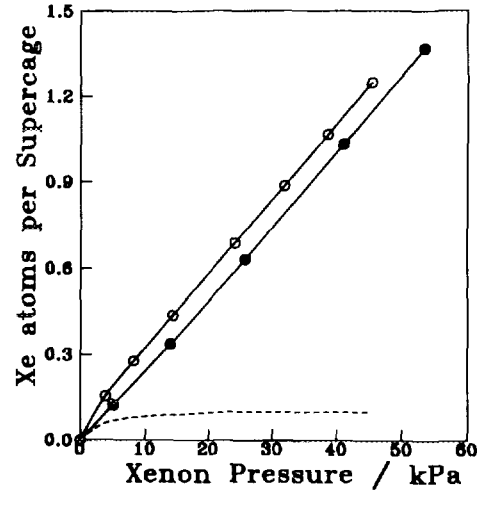

FIG. 10. Xenon adsorption isotherms at 296 K for reduced Ir/NaY–Cl: (○) "clean" sample; (●) after H chemisorption; (---) the difference.

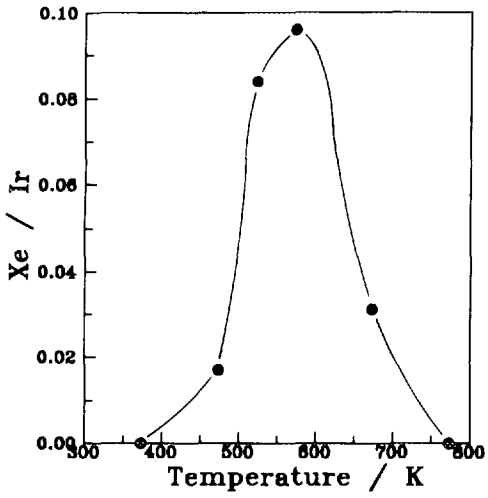

FIG. 11. The xenon adsorption quantity for saturation on Ir/NaY–Cl reduced at 573 K, plotted against the evacuation temperature.

isotherm difference from above ca. 10 kPa to zero pressure. The Xe quantity per total Ir atom can then be plotted against the sample activation temperature, as in Fig. 11. The plot of Xe/Ir vs T_{act} is very similar in shape to the $\Delta\delta$ vs T_{act} plot shown in Fig. 6. This result seems very reasonable because the δ should increase according to the Xe–cluster interaction.

In the same way as for our earlier investigation on Pt/NaY, Pd/NaY, and Ru/NaY, an Ir cluster entrapped in the supercage may be assumed to take a nearly spherical geometry, attached on the wall of the zeolite framework near to as many six-membered oxygen rings as possible. It may further be assumed that at the adsorption saturation the cluster adsorbs a maximum number of xenon atoms that can be in direct contact with the cluster (9, 15). With these assumptions, the number of adsorbed xenon atoms on the cluster consisting of a certain number of Ir atoms can be obtained with space-filling models of xenon atoms and an Ir cluster in the supercage. For example, if a cluster consists of 40 Ir atoms, the number of the adsorbed xenon atoms on the cluster becomes 4 because only one xenon atom can be in direct contact with the cluster through each of the four supercage apertures. The ratio between the 4 adsorbed Xe atoms and the 40 Ir atoms provides 0.1 Xe/Ir for the 40-atom cluster. Extension of this procedure over the range of clusters of 20–50 Ir atoms gave the theoretical curve, shown in Fig. 12, between the Xe/Ir ratio and the number of Ir atoms per cluster. Then, the average number of Ir atoms per cluster for a given sample can be determined from the experimentally measured Xe/Ir ratio to fit for the curve.

Table 3 summarizes the results of xenon adsorption measurement. The average number of Ir atoms per cluster (n) obtained from Ir/NaY–Cl and Ir/NaY–Aq (evacuated at 723 K) was about 50, which is very similar to 1-nm Pt clusters located in the supercages (9, 11). Structural parameters listed in Table 2 include those obtained for Ir/NaY from EXAFS curve-fitting. The results are consistent with the formation of mainly ~1-nm Ir clusters in supercages.

CONCLUSION

In this work, we have investigated details of the precursor treatment effect on the preparation of a small Ir cluster entrapped in the supercage of an NaY zeolite. Clearly, Ir was exchanged as $[Ir(NH_3)_5Cl]^{2+}$ on the NaY zeolite from an aqueous solution of $[Ir(NH_3)_5Cl]Cl_2$. Activation of this iridium species in flowing O_2 prior to reduction with H_2 has been confirmed to be essential for obtaining a small Ir cluster in the zeolite supercages. Our results point out that care should be taken in choosing the activation temperature within a narrow range around 570 K. Otherwise, the Ir dispersion decreased seriously, as Fig. 6 indicated. A maximum Ir dispersion was achieved by performing the subsequent reduction at 573 K. However, the requirement for reduction temperature was much less stringent than that for activation treatment.

EXAFS has clarified that $[Ir(NH_3)_5(H_2O)]^{3+}$ was obtained in NaY zeolite either by stirring the zeolite in an aqueous NH_3 solution of $IrCl_3$ at 330 K over a prolonged period, or by ion exchanging with an aqueous solution of $[Ir(NH_3)_5(H_2O)](ClO_4)_3$. In contrast to $[Ir(NH_3)_5Cl]^{2+}$, this precursor was converted to a small Ir cluster in the supercage by a high-temperature evacuation–reduction proce-

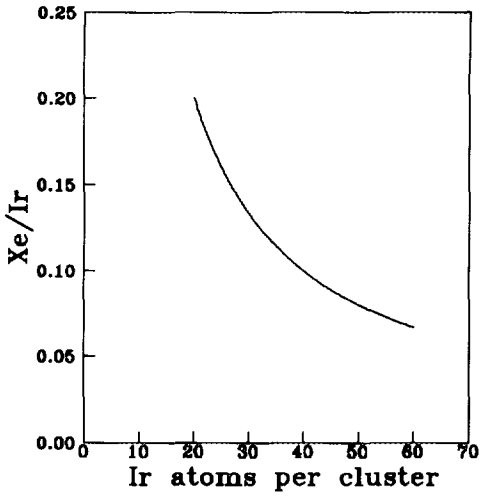

FIG. 12. Xenon atoms per Ir atom plotted against the number of Ir atoms per cluster, obtained from the maximum number of xenon atoms in direct contact with an Ir cluster in a zeolite supercage by using space-filling models of xenon and Ir cluster in the supercage.

dure. When evacuation was performed at 473 K, the resulting cluster size was substantially smaller than the cluster obtained from $[Ir(NH_3)_5Cl]^{2+}$. This method offers the advantage of avoiding an oxidation treatment and eliminating chloride incorporation into the zeolite.

ACKNOWLEDGMENTS

This work was supported by the Korea Science and Engineering Foundation, the Photon Factory (Proposal 92G193), and the Pohang Accelerator Laboratory.

REFERENCES

1. Dufaux, M., Gelin, P., and Naccache, C., *in* "Studies in Surface Science and Catalysis, Vol. 5: Catalysts by Zeolites" (B. Imelik, C. Naccache, Y. Ben Taarit, J. C. Vedrine, G. Coudurier, and H. Praliaud, Eds.), p. 261. Elsevier, Amsterdam, 1980.
2. Gelin, P., Coudurier, G., Ben Taarit, Y., and Naccache, C., *J. Catal.* **70,** 32 (1981).
3. Bischoff, H., Jaeger, N. J., and Schulz-Ekloff, G., *Catal. Today* **8,** 501 (1991).
4. Yang, O. B., Woo, S. I., and Ryoo, R., *J. Catal.* **137,** 357 (1992).
5. Beutel, T., Kawi, S., Purnell, S. K., Knözinger, H., and Gates, B. C., *J. Phys. Chem.* **97,** 7284 (1993).
6. Kawi, S., Chang, J.-R., and Gates, B. C., *J. Catal.* **142,** 585 (1993).
7. Kawi, S., and Gates, B. C., *Catal. Lett.* **10,** 263 (1991).
8. Teo, B. K., "EXAFS: Basic Principles and Data Analysis." Springer-Verlag, New York, 1986.
9. Ryoo, R., Cho, S. J., Pak, C., Kim, J.-G., Ihm, S.-K., and Lee, J. Y., *J. Am. Chem. Soc.* **114,** 76 (1992).
10. Schmidtke, H.-H., *in* "Inorganic Syntheses, Vol. 12" (R. W. Parry, Ed.), p. 243. McGraw–Hill, New York, 1970.
11. Ryoo, R., Cho, S. J., Pak, C., and Lee, J. Y., *Catal. Lett.* **20,** 107 (1993).
12. Newville, M., Livins P., Yacoby, Y., Rehr, J. J., and Stern, E. A., *Phys. Rev. B* **47,** 14126 (1993).
13. Rehr, J. J., Musdre de Leon, J., Zabinski, S. I., and Albers, R. C., *J. Am. Chem. Soc.* **113,** 5135 (1991).
14. Rehr, J. J., Albers, R. C., and Zabinski, S. I., *Phys. Rev. Lett.* **69,** 3397 (1992).
15. Cho, S. J., Jung, S. M., Shul, Y. G., and Ryoo, R., *J. Phys. Chem.* **96,** 9922 (1992).
16. Kim, J.-G., Ihm, S.-K., Lee, J. Y., and Ryoo, R., *J. Phys. Chem.* **95,** 8546 (1991).
17. Rogers, D. B., Shannon, R. D., Sleight, A. W., and Gillson, J. L., *Inorg. Chem.* **8,** 841 (1969).